

Molecular Geometry Prediction using a Deep Generative Graph Neural Network

Elman Mansimov,[†] Omar Mahmood,[‡] Seokho Kang,[¶] and Kyunghyun Cho^{*,†,‡,§,||}

[†]*Department of Computer Science, Courant Institute of Mathematical Sciences, New York University, 60 5th Avenue, New York, New York 10011, United States*

[‡]*Center for Data Science, New York University, 60 5th Avenue, New York, New York 10011, United States*

[¶]*Department of Systems Management Engineering, Sungkyunkwan University, 2066 Seobu-ro, Jangan-gu, Suwon 16419, Republic of Korea*

[§]*Facebook AI Research, 770 Broadway, New York, New York 10003, United States*

^{||}*CIFAR Azrieli Global Scholar, Canadian Institute for Advanced Research, 661 University Avenue, Toronto, ON M5G 1M1, Canada*

E-mail: kyunghyun.cho@nyu.edu

Phone: +1 212 998 3366. Fax: +1 212 995 4121

Abstract

A molecule’s geometry, also known as conformation, is one of a molecule’s most important properties, determining the reactions it participates in, the bonds it forms, and the interactions it has with other molecules. Conventional conformation generation methods minimize hand-designed molecular force field energy functions that are not well correlated with the true energy function of a molecule observed in nature. They generate geometrically diverse sets of conformations, some of which are very similar to the ground-truth conformations and others of which are very different. In this paper we propose a conditional deep generative graph neural network that learns an energy function

from data by directly learning to generate molecular conformations given a molecular graph. On three large scale small molecule datasets, we show that our method generates a set of conformations that on average is far more likely to be close to the corresponding reference conformations than are those obtained from conventional force field methods. Our method maintains geometrical diversity by generating conformations that are not too similar to each other, and is also computationally faster. We also show that our method can be used to provide initial coordinates for conventional force field methods. On one of the evaluated datasets we show that this combination allows us to combine the best of both methods, yielding generated conformations that are on average close to ground-truth conformations with some very similar to ground-truth conformations.

Introduction

The three-dimensional (3-D) coordinates of atoms in a molecule are commonly referred to as the molecule’s geometry or **conformation**. The task, known as conformation generation, of predicting possible valid coordinates of a molecule, is important for determining a molecule’s chemical and physical properties. Conformation generation is also a vital part of applications such as generating 3-D quantitative structure-activity relationships (QSAR), structure-based virtual screening and pharmacophore modeling.¹ Conformations can be determined in a physical setting using instrumental techniques such as X-ray crystallography as well as using experimental techniques. However, these methods are typically time-consuming and costly.

A number of computational methods have been developed for conformation generation over the past few decades¹ and are available in popular open source cheminformatics packages like RDKit.² Typically this problem is approached by using a force field energy function to calculate a molecule’s energy, and then minimizing this energy with respect to the molecule’s coordinates. This hand-designed energy function yields an approximation of the molecule’s true potential energy observed in nature based on the molecule’s atoms, bonds and coordinates. The minimum of this energy function corresponds to the molecule’s most stable

configuration. Although this approach has been commonly used to generate a geometrically diverse set of conformations with certain conformations being similar to ground-truth conformations, it has been shown³ that molecule force field energy functions are a crude approximation of actual molecular energy.

In this paper we propose a deep generative graph neural network that learns the energy function in a data-driven manner. This is done by maximizing the likelihood of the ground-truth conformations of the reference molecules in an end-to-end fashion using back-propagation. We evaluate and compare our method with conventional molecular force field methods on three databases of small molecules by calculating the root-mean-square deviation (RMSD) between generated and ground-truth conformations. We show that conformations generated by our model are on average far more likely to be close to the ground-truth conformation compared to those generated by conventional force field methods *i.e.* the variance of the RMSD between generated and ground-truth conformations is lower for our method. Despite having lower variance, we show that our method does not generate geometrically similar conformations. We also show that our approach is computationally faster than force field methods.

A disadvantage of our model is that in general for a given molecule, the generated conformation by our model most similar to the ground-truth conformation lies further away from the ground-truth conformation than does the conformation most similar to the ground-truth conformation generated by force field methods. We show that for the QM9 small molecule dataset, the best of both methods can be combined by using the conformations generated by the deep generative graph neural network as an initialization to the force field method.

Our source code and preprocessed datasets are available online at <https://github.com/nyu-dl/dl4chem-geometry>.

Conformation Generation

We consider a molecule as an undirected, complete graph $G = (V, E)$, where V is a set of vertices corresponding to atoms, and E is a set of edges representing the interactions between pairs of atoms from V . Each atom is represented as a vector $v_i \in \mathbb{R}^{d_v}$ of node features, and the edge between the i -th and j -th atoms is represented as a vector $e_{ij} \in \mathbb{R}^{d_e}$ of edge features. There are M vertices and $M(M-1)/2$ edges. We define a plausible conformation as one that may correspond to a stable configuration of a molecule. Given the graph of a molecule, the task of molecular geometry prediction is the generation of a set of plausible conformations $X_a = (x_1^a, \dots, x_M^a)$, where $x_i^a \in \mathbb{R}^3$ is a vector of the 3-D coordinates of the i -th atom in the a -th conformation.

Molecules can transition between conformations and end up in different local minima based on the stability of the respective conformations and environmental conditions. As a result, there is more than one plausible conformation associated with each molecule; it is hence natural to formulate conformation generation as finding (local) minima of an energy function $\mathcal{F}(X, G)$ defined on a pair of molecule graph and conformation:

$$\{X_1, \dots, X_S\} = \arg \min_X \mathcal{F}(X, G). \quad (1)$$

Alternatively, we could sample from a Gibbs distribution:

$$\{X_1, \dots, X_S\} \sim p_{\mathcal{F}}(X|G), \quad (2)$$

where

$$p_{\mathcal{F}}(X|G) = \frac{1}{\zeta(G)} \exp \{-\mathcal{F}(X, G)\}, \quad (3)$$

where ζ is a normalizing constant. We use S to indicate the number of conformations we generate from each molecule.

Under this view, the problem of conformation generation is decomposed into two stages. In the first stage, a computationally-efficient energy function $\mathcal{F}(X, G)$ is constructed. The second stage involves either performing optimization as in Eq. (1) or sampling as in Eq. (2) to generate a set of conformations from this energy function.

Energy Function Construction A conventional approach is to define an energy function semi-automatically. The functional form of an energy function is designed carefully to incorporate various chemical properties, whereas detailed parameters of the energy function are either computationally or experimentally estimated. Two widely used energy functions are the Universal Force Field (UFF)⁴ and the Merck Molecular Force Field (MMFF).⁵ In contrast to these methods, here we will describe how to estimate the energy function or probability distribution directly from data using the latest techniques from deep learning.

Energy Minimization/Sampling Once the energy function is defined, a conventional approach is to run the minimization many times starting from different initial conformations. Due to the non-convexity of the energy function, each run is likely to end up in a unique local minimum, allowing us to collect a set of many conformations.

A typical approach is to use distance geometry (DG)⁶ or its variants, such as experimental-torsion basic knowledge distance geometry (ETKDG),⁷ to randomly generate an initial conformation that satisfies various geometric constraints such as lower and upper bounds on the distances between atoms. Starting from the initial conformation, an iterative optimization algorithm, such as L-BFGS,⁸ gradually updates the conformation until it finds a minimum of the energy function. In this paper, we instead propose an approach based on deep generative models that allow us to sample directly from a distribution over all possible conformations given a molecule graph.

Deep Generative Model for Molecular Geometry

We propose to “learn” an energy function $\mathcal{F}(G, X)$ from a database containing many pairs of a molecule and its experimentally obtained conformation. Let $\mathcal{D} = \{(G_1, X_1^*), \dots, (G_N, X_N^*)\}$ be a set of examples from such a database, where X_n^* is “a” ground-truth conformation, often experimentally obtained or verified. Learning an energy function can then be expressed as the following optimization problem:

$$\hat{\mathcal{F}}(G, X) = \arg \max_{\mathcal{F}} \frac{1}{N} \sum_{n=1}^N \underbrace{\log p_{\mathcal{F}}(X_n^* | G_n)}_{(a)}, \quad (4)$$

where $p_{\mathcal{F}}$ is a Gibbs distribution defined using \mathcal{F} as in Eq. (3). In other words, we can learn the energy function \mathcal{F} by maximizing the log-likelihood of the data D .

Conditional Variational Graph Autoencoders

We use a conditional version of a variational autoencoder⁹ to model the distribution $p_{\mathcal{F}}$ in Eq. (4) (a). This choice enables an underlying model to capture the complicated, multi-modal nature of this distribution, while allowing us to efficiently sample from this distribution. This is done by introducing a set of latent variables $Z = \{z_1, \dots, z_M\}$, where $z_m \in \mathbb{R}^{d_z}$ and rewriting the conditional log-probability $\log p_{\mathcal{F}}(X|G)$ as

$$\log p(X|G) = \log \int p(X|Z, G)p(Z|G)dZ, \quad (5)$$

where we omit the subscript \mathcal{F} for brevity.

The marginal log-probability in Eq. (5) is generally intractable to compute, and we instead maximize the stochastic approximation to its lower bound, as is standard practice

in problems involving variational inference:

$$\log p(X|G) \geq \mathbb{E}_{Z \sim Q(Z|G, X)} [\underbrace{\log p(X|Z, G)}_{\text{(b) likelihood}}] - \text{KL}(\underbrace{Q(Z|G, X)}_{\text{(c) posterior}} \parallel \underbrace{P(Z|G)}_{\text{(a) prior}}) \quad (6)$$

$$\approx \frac{1}{K} \sum_{k=1}^K \log p(X|Z^k, G) - \text{KL}(Q(Z|G, X) \parallel P(Z|G)), \quad (7)$$

where Z^k is the k -th sample from the (approximate) posterior distribution Q above. We assume that we can compute the KL divergence analytically, for instance by constructing Q and P to be normal distributions.

Modeling the Graph using a Message Passing Neural Network We use a message passing neural network (MPNN)¹⁰, a variant of a graph neural network,^{11,12} which operates on a graph G directly and is invariant to graph isomorphism. The MPNN consists of L layers. At each layer l , we update the hidden vector $h(v_i) \in \mathbb{R}^{d_h}$ of each node and hidden matrix $h(e_{ij}) \in \mathbb{R}^{d_h \times d_h}$ of each edge using the equation

$$h^l(v_i) = \text{GRU}(h^{l-1}(v_i), J(h^{l-1}(v_i), h^{l-1}(v_{j \neq i}), h(e_{i,j \neq i}))), \quad (8)$$

where J is a linear one layer neural network that aggregates the information from neighboring nodes according to its hidden vectors of respective nodes and edges. GRU is a gated recurrent network that combines the new aggregate information and its corresponding hidden vector from previous layer¹³. The weights of the message passing function J and GRU are shared across the L layers of the MPNN.

Prior Parameterization We use the MPNN described above to model the prior distribution $P(Z|G)$ in Eq. (6) (a). We initialize $h^0(v_i)$ and $h(e_{ij})$ in Eq. (8) as linear transformations

of the feature vectors v_i and e_{ij} of the nodes and edges respectively:

$$h^0(v_i) = U_{\text{node}}^{\text{prior}} v_i; \quad h(e_{ij}) = U_{\text{edge}}^{\text{prior}} e_{ij}, \quad (9)$$

where $U_{\text{node}}^{\text{prior}}$ and $U_{\text{edge}}^{\text{prior}}$ are matrices representing the linear transformations for the nodes and edges respectively. The final hidden vector $h^L(v_i)$ of each node is passed through a two layer neural network with hidden size d_f , whose output $\tilde{h}^L(v_i)$ is transformed into the mean and variance vectors of a Normal distribution with a diagonal covariance matrix:

$$\mu_i = W_{\mu}^{\text{prior}} \tilde{h}^L(v_i) + b_{\mu}^{\text{prior}}; \quad (10)$$

$$\sigma_i^2 = \exp \left\{ W_{\sigma}^{\text{prior}} \tilde{h}^L(v_i) + b_{\sigma}^{\text{prior}} \right\}, \quad (11)$$

where W_{μ}^{prior} and $W_{\sigma}^{\text{prior}}$ are the weight matrices and b_{μ}^{prior} and $b_{\sigma}^{\text{prior}}$ are the bias terms of the transformations. These are used to form the prior distribution:

$$\log P(Z|G) = \sum_{i=1}^N \sum_{j=1}^3 -\frac{(\mu_{i,j} - z_{i,j})^2}{2\sigma_{i,j}^2} - \log \sqrt{2\pi\sigma_{i,j}^2}, \quad (12)$$

where $\mu_{i,j}$ and $\sigma_{i,j}^2$ are the j -th components of the mean and variance vectors respectively. In other words, we parameterize the prior distribution as a factorized Normal distribution factored over the vertices and the dimensions in the 3-D coordinate.

Likelihood Parameterization We use a similar MPNN to model the likelihood distribution, $P(X|Z, G)$ in Eq. (6) (b). The only difference is that this distribution is conditioned not only on the molecular graph $G = (V, E)$ but also on the latent set $Z = \{z_1, \dots, z_M\}$. We incorporate the latent set Z by adding the linear transformation of the node feature vector v_i to its corresponding latent variable z_i . This result is used to initialize the hidden vector:

$$h^0(v_i) = U_{\text{node}}^{\text{likelihood}} v_i + z_i; \quad h(e_{ij}) = U_{\text{edge}}^{\text{likelihood}} e_{ij}, \quad (13)$$

where $U_{\text{node}}^{\text{likelihood}}$ and $U_{\text{edge}}^{\text{likelihood}}$ are matrices representing the linear transformations for the nodes and edges respectively. From there on, we run neural message passing as in Eqs. (8–11), with a new set of parameters, $\theta_{\text{likelihood}}$, $W_{\mu}^{\text{likelihood}}$, $b_{\mu}^{\text{likelihood}}$, $W_{\sigma}^{\text{likelihood}}$ and $b_{\sigma}^{\text{likelihood}}$. The final mean and variance vectors are now three dimensional, representing the 3-D coordinates of each atom, and we can compute the log-probability of the coordinates using Eq. (12).

Posterior Parameterization As computing the exact posterior $P(Z|G, X)$ is intractable, we resort to amortized inference using a parameterized, approximate posterior $Q(Z|G, X)$ in Eq. (6) (c). We use a similar approach to our parameterization of the prior distribution above. However, we replace the input to the MPNN with the concatenation of an edge feature vector e_{ij} and the corresponding distance (proximity) matrix $D(X^*)$ of the ground-truth 3-D conformation X^* :

$$h(e_{ij}) = U_{\text{edge}}^{\text{posterior}} \begin{bmatrix} e_{ij} \\ D(x_i^*) \end{bmatrix}. \quad (14)$$

With a new set of parameters, $\theta_{\text{posterior}}$, $W_{\mu}^{\text{posterior}}$, $b_{\mu}^{\text{posterior}}$, $W_{\sigma}^{\text{posterior}}$ and $b_{\sigma}^{\text{posterior}}$, the MPNN outputs a Normal distribution for each latent variable z_i . Linear weight embeddings of nodes U_{node} are shared between prior, likelihood and posterior.

Training the Conditional Variational Graph Autoencoder

With the choice of the Gaussian latent variables z_i , we can use the reparameterization trick⁹ to compute the gradient of the stochastic approximation to the lower bound in Eq. (7) with respect to all the parameters of the three distributions⁹. This property allows us to train this model on a large dataset using stochastic gradient descent (SGD). However, there are two major considerations that must be made before training this model on a large molecule database.

(1) Post-Alignment Likelihood An important property of conformation generation over a usual problem of regression is that we must take into account rotation and translation. Let R be an alignment function that takes as input a target conformation and a predicted conformation, aligns the reference conformation to the predicted conformation and returns the aligned reference conformation. $\hat{X} = R(X, X^*)$ is the conformation obtained by rotating and translating the reference conformation X^* to have the smallest distance to the predicted conformation X according to a predefined metric such as RMSD:

$$\text{RMSD}(\hat{X}, X^*) = \sqrt{\frac{1}{M} \sum_{i=1}^M \|\hat{x}_i - x_i^*\|^2}. \quad (15)$$

This alignment function R is selected according to the problem at hand, and we present below its use in a general form without exact specification.

We implement this invariance to rotation and translation by parameterizing the output of the likelihood distribution above to be aligned to the target molecule. That is,

$$\log p(X|G, Z) = \sum_{i=1}^M \sum_{j=1}^3 -\frac{(\mu_{i,j} - \hat{x}_{i,j}^*)^2}{2\sigma_{i,j}^2} - \log \sqrt{2\pi\sigma_{i,j}^2}, \quad (16)$$

where \hat{x}_i^* is the coordinate of the i -th atom aligned to the mean conformation $\{\mu_1, \dots, \mu_N\}$. That is,

$$\{\hat{x}_1^*, \dots, \hat{x}_M^*\} = R(\{\mu_1, \dots, \mu_M\}, X^*). \quad (17)$$

In other words, we rotate and translate the reference conformation X^* to be best aligned to the predicted conformation (or its mean) before computing the log-probability. This encourages the model to assign high probability to a conformation that is easily aligned to the reference conformation X^* , which is precisely the goal of maximum log-likelihood.

(2) Unconditional Prior Regularization The second term in the lower bound in Eq. (6), which is the KL divergence between the approximate posterior and prior, does not have a point minimum but an infinitely long valley consisting of minimum values. Consider the KL divergence between two univariate Normal distributions:

$$\text{KL}(\mathcal{N}(\mu_1, \sigma_1^2) \parallel \mathcal{N}(\mu_2, \sigma_2^2)) = \log \frac{\sigma_2}{\sigma_1} + \frac{\sigma_1^2 + (\mu_1 - \mu_2)^2}{2\sigma_2^2} - \frac{1}{2}. \quad (18)$$

When both distributions are shifted by the same amount, the KL divergence remains unchanged. This could lead to a difficulty in optimization, as the means of the posterior and prior distributions could both diverge.

In order to prevent this pathological behavior, we introduce an unconditional prior distribution $P(Z)$ which is a factorized Normal distribution:

$$P(Z) = \prod_{i=1}^M \mathcal{N}(z_i | 0, I), \quad (19)$$

where \mathcal{N} computes a Normal probability density, and I is a $d_z \times d_z$ identity matrix. We minimize the KL divergence between the original prior distribution $P(Z|G)$ and this unconditional prior distribution $P(Z)$ in addition to maximizing the lowerbound, leading to the following final objective function for each molecule:

$$\mathcal{L} = \log p(X|Z^1, G) - \text{KL}(Q(Z|G, X) \parallel P(Z|G)) - \alpha \cdot \text{KL}(P(Z|G) \parallel P(Z)), \quad (20)$$

where we assume $K = 1$ and introduce a coefficient $\alpha \geq 0$.

Inference: Predicting Molecular Geometry

Learning a conditional variational autoencoder above corresponds to the first stage of conformation generation, that is, the stage of energy function construction. Once the energy function is constructed, we need to sample multiple conformations from the Gibbs distribu-

tion defined using the energy function, which is $\log P(X|G)$ in Eq. (5). Our parameterization of the Gibbs distribution using a directed graphical model¹⁴ allows us to efficiently sample from this distribution. We first sample from the prior distribution, $\tilde{Z} \sim P(Z|G)$, and then sample from the likelihood distribution, $\tilde{X} \sim P(X|\tilde{Z}, G)$. In practice, we fix the output variance $\sigma_{i,j}$ of the likelihood distribution to be 1 and take the mean set $\{\mu_1, \dots, \mu_M\}$ as a sample from the model.

Experimental Setup

Data

We experimentally verify the effectiveness of the proposed approach using three databases of molecules: QM9,^{15,16} COD¹⁷ and CSD.¹⁸ These datasets are selected as they possess distinct properties from each other, which allows us to carefully study various aspects of the proposed approach. Although, there is an overlap between COD and CSD databases, since both of these databases were based on published crystallography data. We only keep molecules from each database that can be processed by RDKit¹. We further remove disconnected compounds *i.e.* those whose Simplified Molecular-Input Line-Entry System¹⁹ (SMILES) representation contains ‘.’. See Fig. 1 for some other properties of these three datasets.

QM9 The filtered QM9 dataset contains 133,015 molecules, each of which contains up to 9 heavy atoms of types C, N, O and F. Each molecule is paired with a ground-truth conformation obtained by optimizing the molecular geometry with density functional theory (DFT) at the B3LYP/6-31G(2df,p) level of theory, which implies that these ground-truth conformations may not necessarily correspond to the lowest energy configurations of the molecules. We hold out separate 5,000 and 5,000 randomly selected molecules as validation and test sets, respectively.

¹ Version 2018.09.1

COD We use the organic part of the COD dataset. We further filter out any molecule that contains more than 50 heavy atoms of types B, C, N, O, F, Si, P, S, Cl, Ge, As, Se, Br, Te and I. This results in 66,663 molecules, out of which we hold out separate 3,000 and 3,000 randomly selected ones respectively for validation and test purposes. Ground-truth conformations are voluntarily contributed to the dataset and are often determined either experimentally or by DFT.²⁰

CSD Similarly to COD, we remove any molecule that contains more than 50 heavy atoms, resulting in a total of 236,985 molecules. This dataset contains organic and metal-organic crystallographic structures which have been verified experimentally.¹⁸ The atom types in this dataset are S, N, P, Be, Tc, Xe, Br, Rh, Os, Zr, In, As, Mo, Dy, Nb, La, Te, Th, Ga, Tl, Y, Cr, F, Fe, Sb, Yb, Tb, Pu, Am, Re, Eu, Hg, Mn, Lu, Nd, Ce, Ge, Sc, Gd, Ca, Ti, Sn, Ir, Al, K, Tm, Ni, Er, Co, Bi, Pr, Rb, Sm, O, Pt, Hf, Se, Np, Cd, Pd, Pb, Ho, Ag, Mg, Zn, Ta, V, B, Ru, W, Cl, Au, U, Si, Li, C and I. We hold out separate 3,000 and 3,000 randomly selected molecules for validation and test purposes respectively.

Models

Baselines As a point of reference, we minimize a force field starting from a conformation created using ETKDG.⁷ We test both UFF and MMFF, and respectively call the resulting approaches **ETKDG+UFF** and **ETKDG+MMFF**. We use the implementations in RDKit with the default hyperparameters.²

Conditional Variational Graph Autoencoder We build one conditional variational graph autoencoder for each dataset. We use $d_h = 50$ hidden units at each layer of neural message passing (Eq. 8) in each of the three MPNNs corresponding to the prior, likelihood and posterior distributions. We use $d_f = 100$ in the two layer neural network that comes after the MPNN. As described earlier, we fix the variance of the output in the likelihood distribution to 1. We use $L = 3$ layers per network for QM9 and $L = 5$ layers per network

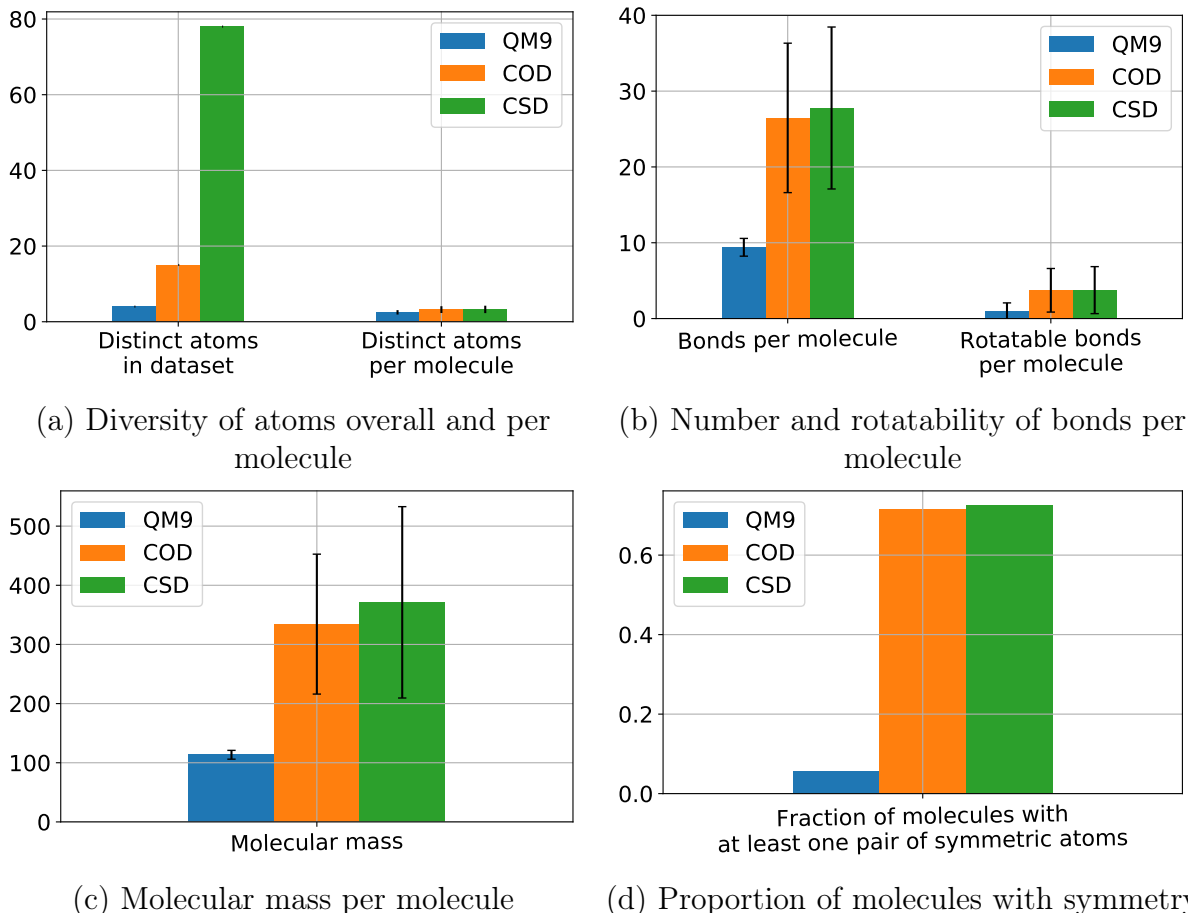


Figure 1: Dataset Characteristics: information regarding the atoms, bonds, molecular mass and symmetry of molecules in each dataset.

for COD and CSD. We chose these hyperparameter values by carrying out a grid-search and choosing the values that had the best performance on the validation set. The grid-search procedure and the performance of models with different hyperparameters are shown in the Appendix .

Learning For all models, we use dropout²¹ at each layer of the neural network that comes after the MPNN with a dropout rate of 0.2 to regularize learning. We set the coefficient α in Eq. (20) to 10^{-5} . We train each model using Adam²² with a fixed learning rate of 3×10^{-4} . All models were trained with a batch size of 20 molecules on 1 Nvidia GPU with 12 GB of RAM.

Inference There are two modes of inference with the proposed approach. The first approach is to sample from a trained conditional variational graph autoencoder by first sampling from the prior distribution and taking the mean vectors from the likelihood distribution; we refer to this as **CVGAE**. We can then use these samples further as initializations of MMFF minimization; we refer to this as **CVGAE+MMFF**. The latter approach can be thought of as a trainable approach to initializing a conformation in place of DG or ETKDG.

Evaluation

In principle, the quality of the sampled conformations should be evaluated based on their molecular energies, for instance by DFT, which is often more accurate than force field methods.³ However, the computational complexity of the DFT calculation is superlinear with respect to the number of electrons in a molecule, and so is often impractical.²³ Instead, we follow prior work on conformation generation²⁴ and evaluate the baselines and proposed method using the RMSD (Eq. 15) of the heavy atoms between a ground-truth conformation and a predicted conformation which is fast and simple to calculate.

Results

When evaluating each method, we first sample 100 conformations per molecule for each method in the test set. We can make several observations from Table 1. First, compared to other methods, our proposed CVGAE always succeeds at generating the specified number of conformations for any of the molecules in the test set. Since all other evaluated approaches were unsuccessful at generating at least one conformation for a very small number of test molecules, we report results for the molecules for which all evaluated methods generated at least one conformation. We report the *median* of the mean of the RMSD, the *median* of the standard deviation of the RMSD and the *median* of the best (lowest) RMSD among all generated conformations for each test molecule. Across all three datasets, every evaluated

Table 1: Number of successfully processed molecules in the test set (success per test set \uparrow), number of successfully generated conformations out of 100 (success per molecule \uparrow), median of mean RMSD (mean \downarrow), median of standard deviation of RMSD (std. dev. \downarrow) and median of best RMSD (best \downarrow) per molecule on QM9, COD and CSD datasets. ETKDG stands for Distance Geometry with experimental torsion-angle preferences. UFF and MMFF are force field methods and stand for Universal Force Field and Molecular Mechanics Force Field respectively. CVGAE stands for Conditional Variational Graph Autoencoder. CVGAE + Force Field represents running the MMFF force field optimization initialized by CVGAE predictions.

Dataset		ETKDG + Force Field UFF	ETKDG + Force Field MMFF	CVGAE	CVGAE + Force Field MMFF
QM9	success per test set	96.440%	96.440%	100%	99.760%
	success per molecule	98.725%	98.725%	100%	98.684%
	mean	0.425	0.415	0.390	0.367
	std. dev.	0.176	0.189	0.017	0.074
	best	0.126	0.092	0.325	0.115
COD	success per test set	99.133%	99.133%	100%	95.367%
	success per molecule	99.627%	99.627%	100%	99.071%
	mean	1.389	1.358	1.331	1.656
	std. dev.	0.407	0.415	0.099	0.425
	best	0.429	0.393	1.206	0.635
CSD	success per test set	97.400%	97.400%	100%	99.467%
	success per molecule	99.130%	99.130%	100%	97.967%
	mean	1.537	1.488	1.506	1.833
	std. dev.	0.421	0.418	0.115	0.434
	best	0.508	0.478	1.343	0.784

method achieves roughly the same median of the mean RMSD. More importantly, the standard deviation of the RMSD achieved by CVGAE is *significantly* lower than that achieved by ETKDG + Force Field. After the initial generation stage, conformations are usually further evaluated and optimized by running the computationally expensive DFT optimization. Reducing the standard deviation can lower the number of conformations on which DFT optimization has to be run in order to achieve a valid conformation. On the other hand, the best RMSD achieved by ETKDG + UFF/MMFF methods is lower than that achieved by CVGAE. Using MMFF initialized by CVGAE (CVGAE + MMFF) instead of ETKDG (ETKDG + MMFF) improves the mean results on the QM9 dataset for CVGAE, and yields

Table 2: Conformation Diversity. Mean and std. dev. represents the corresponding mean and standard deviation of pairwise RMSD between at most 100 generated conformations per molecule.

Dataset		ETKDG + MMFF	CVGAE	CVGAE + MMFF
QM9	mean	0.400	0.106	0.238
	std. dev.	0.254	0.061	0.209
COD	mean	1.148	0.239	1.619
	std. dev.	0.699	0.181	0.537
CSD	mean	1.244	0.567	1.665
	std. dev.	0.733	0.339	0.177

a lower standard deviation and similar best RMSD compared to ETKDG + MMFF. Unfortunately, CVGAE + MMFF worsens the results achieved by CVGAE alone on the COD and CSD datasets.

We also report the diversity of conformations generated by all evaluated methods in Table 2. Diversity is measured by calculating the mean and standard deviation of the pairwise RMSD between each pair of generated conformations per molecule. Overall, we can see that despite having a smaller median of standard deviation of RMSD between generated conformations and ground-truth conformations, CVGAE does not collapse to generating extremely similar conformations. Although, CVGAE generates relatively less diverse samples compared to ETKDG + MMFF baseline on all datasets. The conformations of molecules generated by CVGAE + MMFF are less diverse on the QM9 dataset and more diverse on COD/CSD datasets compared to ETKDG + MMFF baseline.

The computational efficiency of each of the evaluated approaches on the QM9 and COD datasets is shown in Figure 2. For consistency, we generated one conformation for one molecule at a time using each of the evaluated methods on an Intel(R) Xeon(R) E5-2650 v4 CPU. On the QM9 dataset, CVGAE is $2\times$ more efficient than ETKDG + UFF/MMFF, while CVGAE + MMFF is slightly slower than ETKDG + UFF/MMFF. On the COD dataset, which contains a larger number of atoms per molecule, CVGAE is almost $10\times$ as

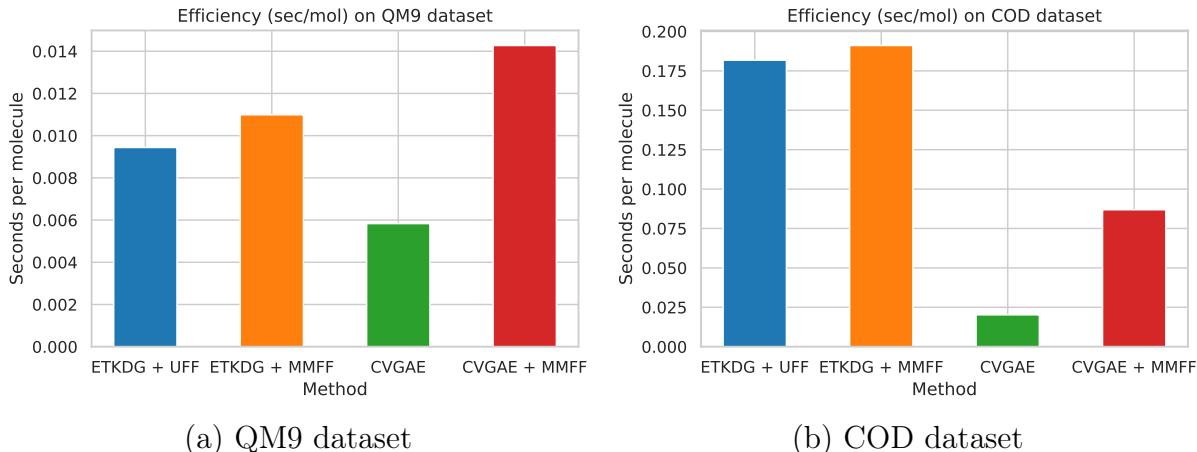


Figure 2: Computational efficiency of various approaches on QM9 and COD datasets

fast as ETKDG + UFF/MMFF, while CVGAE + MMFF is about $2\times$ as fast as ETKDG + UFF/MMFF. This shows that CVGAE scales much better than the baseline ETKDG + UFF/MMFF methods as the size of the molecule grows.

Figures 3 and 4 visualize the median, standard deviation and best RMSD results as a function of the number of heavy atoms in a molecule on the QM9 and COD/CSD datasets respectively. For all approaches, we can see that the best and median RMSD both increase with the number of heavy atoms. The standard deviation of the median RMSD for CVGAE and CVGAE + MMFF is lower than that for ETKDG + MMFF across molecules of almost all sizes. The standard deviation of the best RMSD is slightly higher for CVGAE and CVGAE + MMFF than for ETKDG + MMFF on molecules with at most 12 atoms, but is lower for larger atoms, particularly for CVGAE. Overall, CVGAE yields a lower or similar median RMSD compared to ETKDG + CVGAE across molecules of all sizes but a lower standard deviation, whereas ETKDG + MMFF provides a lower best RMSD particularly for larger molecules observed in the COD/CSD datasets.

Figures 5 and 6 qualitatively compare the results of CVGAE against MMFF and CVGAE + MMFF against CVGAE respectively. For each dataset, each figure shows the three molecules for which the first method in each figure outperforms the second method by the greatest amount, and the three molecules for which the second method outperforms the first

by the greatest amount. The reference molecules are shown alongside the conformations resulting from each of the methods for comparison.

We can see some general trends from both these figures. The conformations produced by the neural network are qualitatively much more similar to the reference in the case of the QM9 dataset than in the cases of the COD and CSD datasets. In the case of the COD and CSD datasets, the CVGAE predictions appear to be squashed or compressed in comparison to the reference molecules. For example, in almost every case we can see the absence of visible rings and the absence of bonds protruding from the lengthwise dimension of the molecule. At the same time we can see that on COD and CSD, CVGAE does better than ETKDG + MMFF in cases where ETKDG + MMFF creates loops and protrusions in the wrong places.

Analysis and Future Work

Overall we observe that CVGAE performs better than ETKDG + MMFF on QM9 than on COD and CSD. One possible reason that could explain this phenomena is that COD and CSD contain much larger number of heavy atoms per molecule than QM9. In the absence of adequate number of neural message passing steps and adequate number of hidden units, the network may converge to outputting a conformation that contains atoms largely along a single non-linear dimension in order to minimize outliers, which would be heavily penalized by the sum of squared distances term in the loss function. A neural network architecture with a larger number of neural message passing steps and larger number of hidden units may be needed to generate less conservative conformations and achieve comparable results to those for QM9. This is a recommended direction of future work that will require more computational resources, including distributed training on multiple GPUs with sufficient memory.

We also observe that our CVGAE method has a lower variance than the baseline methods, so a relatively small number of samples needs to be taken before getting a conformation

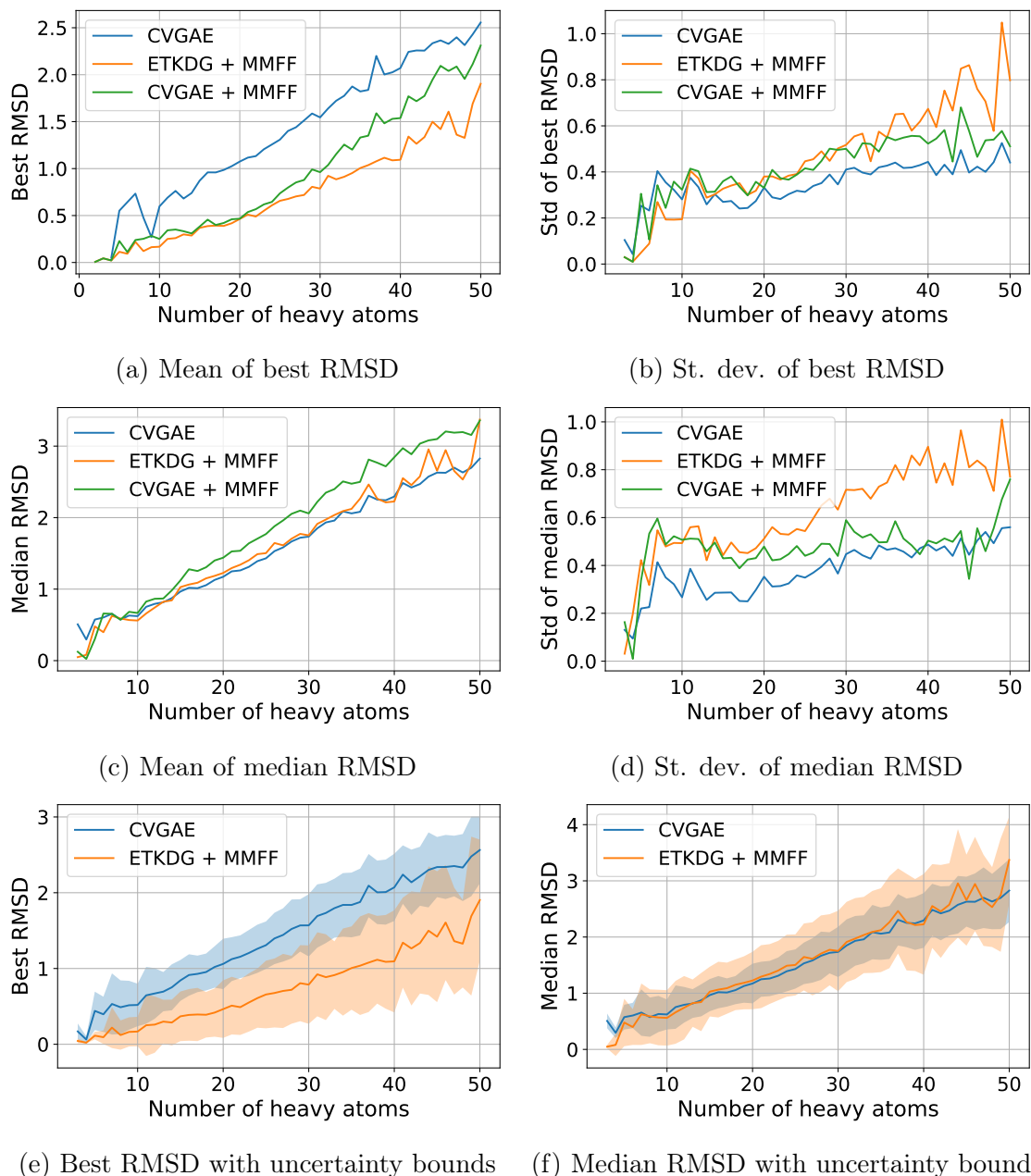


Figure 3: This figure shows the means and standard deviations of the best and median RMSDs on the union of COD and CSD datasets as a function of number of heavy atoms. The molecules were grouped by number of heavy atoms, and the mean and standard deviation of the median and best RMSDs were calculated for each group to obtain these plots. Groups at the left hand side of the graph with less than 1% of the mean number of molecules per group were omitted.

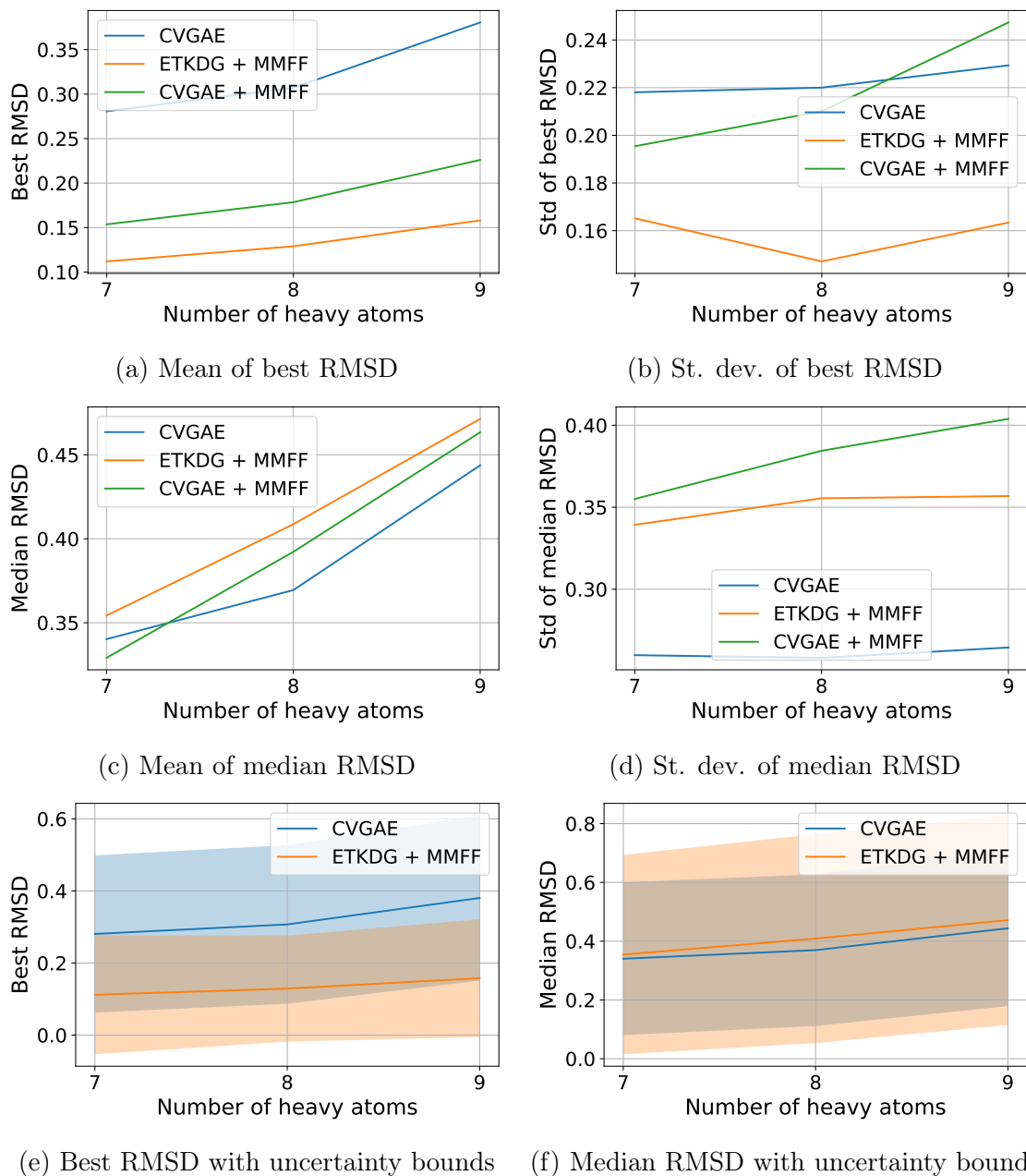


Figure 4: This figure shows the means and standard deviations of the best and median RMSDs on the QM9 dataset as a function of number of heavy atoms. The molecules were grouped by number of heavy atoms, and the mean and standard deviation of the median and best RMSDs were calculated for each group to obtain these plots. Groups at the left hand side of the graph with less than 1% of the mean number of molecules per group were omitted.

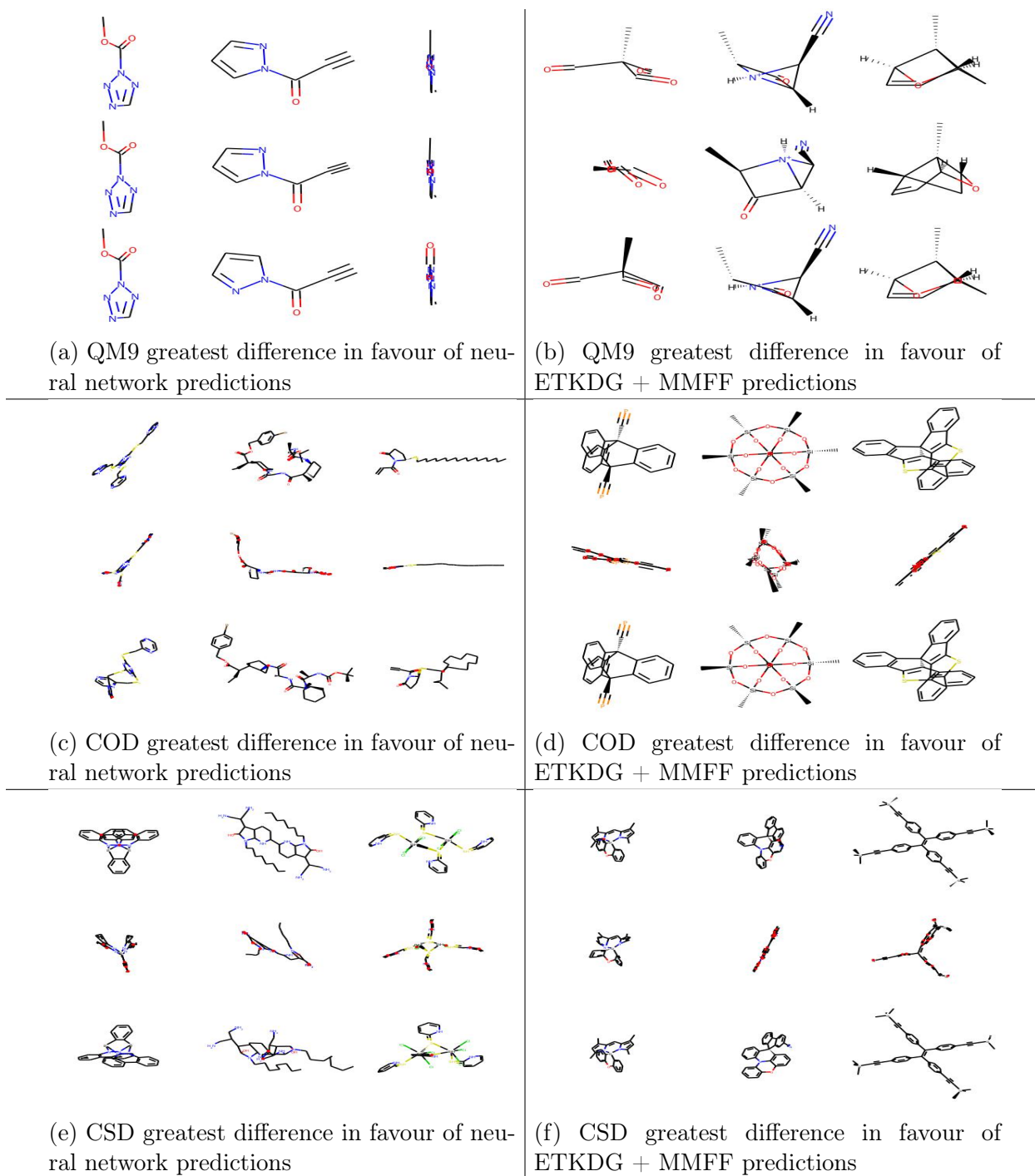


Figure 5: This figure shows the three molecules in each dataset for which the differences between the RMSDs of the neural network predictions and the baseline MMFF predictions were greatest in favour of the neural network predictions ($\max(RMSD_{CVGAE} - RMSD_{ETKDG+MMFF})$), and the three for which this difference was greatest in favour of the ETKDG + MMFF predictions ($\max(RMSD_{ETKDG+MMFF} - RMSD_{CVGAE})$). The top row of each subfigure contains the reference molecules, the middle row contains the neural network predictions and the bottom row contains the conformations generated by applying MMFF to the reference conformations.

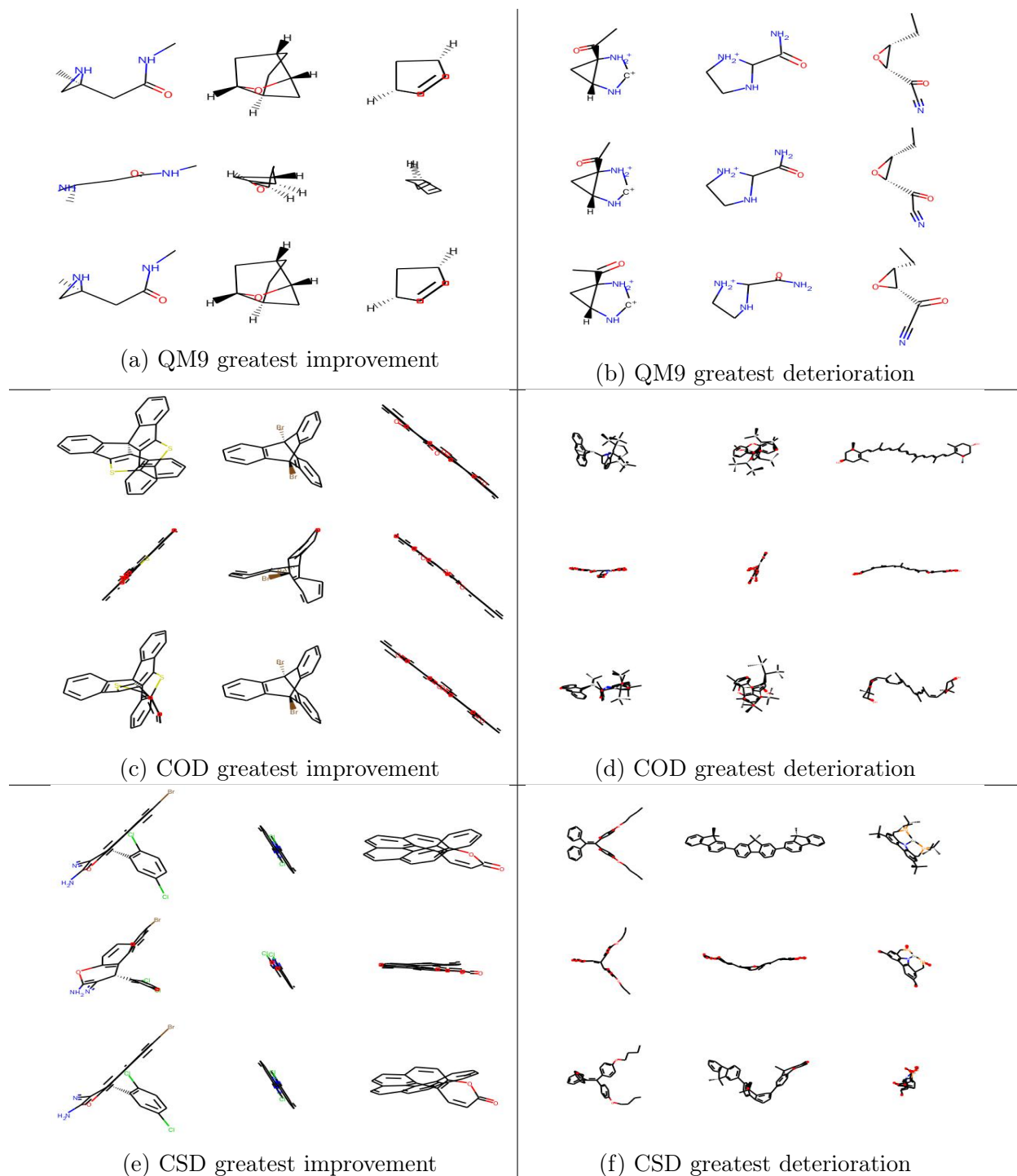


Figure 6: This figure shows the three molecules in each dataset whose RMSD decreased the most and the three whose RMSD increased the most on applying MMFF to the conformations predicted by the neural network. The top row of each subfigure contains the reference molecules, the middle row contains the neural network predictions and the bottom row contains the conformations generated by applying MMFF to the neural network predictions.

with a good RMSD. In addition, CVGAE is faster than force field methods and uses less computational resources once trained. Using conformations generated by CVGAE as an initialization to force field method showed promising results on the QM9 dataset that allowed to combine the best of two distinct methods. However, applying a force field method on the conformations generated by CVGAE leads to an increase in RMSD on the COD and CSD datasets - future work could explore why this is the case. Another avenue of future inquiry could be the joint training of CVGAE and a force field method, which would involve implementing force field minimization using a deep learning framework, connecting this to CVGAE and backpropagating through this aggregate model. This joint training could further yield better results than either method alone.

Acknowledgement

Seokho Kang was supported by the National Research Foundation of Korea (NRF) grant funded by the Korea government (MSIT; Ministry of Science and ICT) (No. NRF-2017R1C1B5075685). Kyunghyun Cho thanks support by eBay, TenCent, NVIDIA and CIFAR.

Conflict of Interest

The authors declare no competing financial interest.

Appendix

Hyperparameter Search

Below are the hyperparameters we tried for the QM9 and COD datasets. We picked the hyperparameters to ensure that a model trained with a batch size of 20 molecules could fit on 1 GPU with 12 GB of RAM.

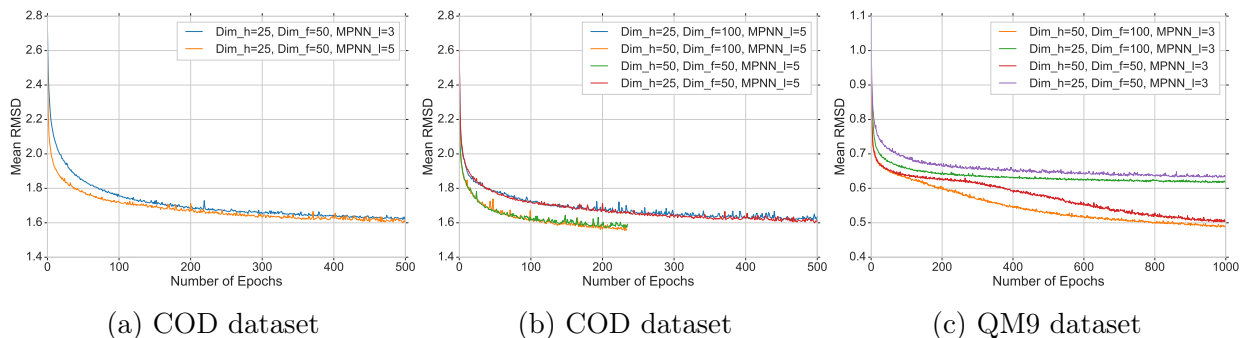


Figure 7: Investigation of number of different hyperparameters on QM9 and COD datasets over different number of epochs. Mean RMSD over number of epochs of best performing model on valid set of corresponding dataset. Mean RMSD was calculated given 10 conformations per molecule.

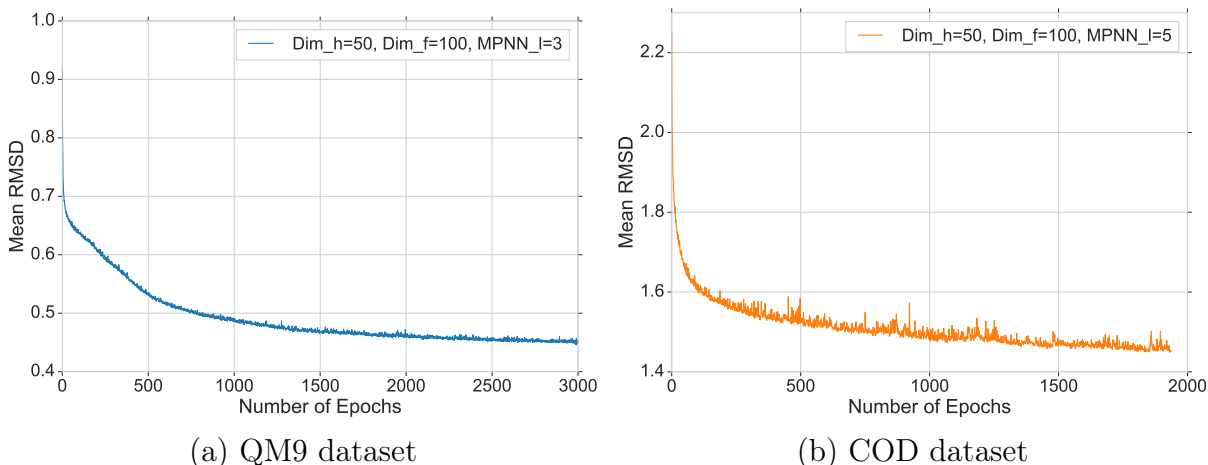


Figure 8: Performance of the best performing model over the number of epochs. Mean RMSD over number of epochs of best performing model on valid set of corresponding dataset. Mean RMSD was calculated given 10 conformations per molecule.

We experimented with the following values of hyperparameters on the QM9 dataset: $d_h = [25, 50]$, $d_f = [50, 100]$. The number of MPNN layers L was fixed to 3 according to previous preliminary experiments. On Figure 7c we can see that the model with $d_h = 50$ and $d_f = 100$ significantly outperforms models with a smaller number of hidden units.

On the COD dataset we experimented with the following values of hyperparameters: $d_h = [25, 50]$, $d_f = [50, 100]$ and number of MPNN layers $L = [3, 5]$. In Figure 7a we can see that the model with 5 MPNN layers slightly outperforms the model with 3 MPNN layers. Similarly to the QM9 dataset, we can see in Figure 7b that a larger number of hidden units

Table 3: Node features.

feature	type	dimension
atom type	one-hot (possible heavy atoms)	vary
atomic number	integer	1
chirality	one-hot (R, S)	2
is aromatic	binary	1
hybridization	one-hot (sp, sp ² , sp ³ , sp ³ d ¹ , sp ³ d ²)	5
degree	integer	1
formal charge	integer	1
no. hydrogens	integer	1
no. radical electrons	integer	1
implicit valence	integer	1
no. rings for each ring size	integer (ring sizes 3, 4, 5, 6, 7, 8)	6
total		> 20

Table 4: Edge features.

feature	type	dimension
bond type (if bond)	one-hot (single, double, triple, aromatic)	4
stereochemistry (if bond)	one-hot (E, Z)	2
is conjugated (if bond)	binary	1
is in ring (if bond)	binary	1
is in same ring	binary	1
graph distance (shortest path)	integer	1
total		10

results in significantly faster convergence and better performance.

We selected the model with the best hyperparameter values given by our grid-search. Figure 8 shows the RMSD of this model on the validation set as a function of number of epochs on the QM9 and COD datasets.

Molecular Features

To represent molecules as graph-structured data, each of the nodes and edges in the molecule is represented using the features described in Tables 3 and 4, according to related literature.^{10,25,26} We only consider heavy atoms, and do not consider hydrogen atoms as explicit nodes *i.e.* hydrogen atoms are represented as part of the input features and their coordinates are not predicted by the neural network. In Table 4, the first four edge features are only

calculable if the corresponding atom pair is bonded, while the last two edge features are calculable for every atom pair. All features are generated using RDKit.²

References

- (1) Schwab, C. H. Conformations and 3D Pharmacophore Searching. *Drug Discov. Today* **2010**, *7*, e245–e253.
- (2) Landrum, G. RDKit: Open-Source Cheminformatics. <http://www.rdkit.org>, (accessed December 18, 2018).
- (3) Kanal, I. Y.; Keith, J. A.; Hutchison, G. R. A Sobering Assessment of Small-Molecule Force Field Methods for Low Energy Conformer Predictions. *Int. J. Quantum Chem.* **2017**, *118*, e25512.
- (4) Rappé, A. K.; Casewit, C. J.; Colwell, K. S.; Goddard III, W. A.; Skiff, W. M. UFF, A Full Periodic Table Force Field for Molecular Mechanics and Molecular Dynamics Simulations. *J. Am. Chem. Soc.* **1992**, *114*, 10024–10035.
- (5) Halgren, T. A. Merck Molecular Force Field. I. Basis, Form, Scope, Parameterization, and Performance of MMFF94. *J. Comput. Chem.* **1996**, *17*, 490–519.
- (6) Blaney, J. M.; Dixon, J. S. Distance Geometry in Molecular Modeling. *Rev. Comput. Chem.* **1994**, 299–335.
- (7) Riniker, S.; Landrum, G. A. Better Informed Distance Geometry: Using What We Know To Improve Conformation Generation. *J. Chem. Inf. Model.* **2015**, *55*, 2562–2574.
- (8) Liu, D. C.; Nocedal, J. On the Limited Memory BFGS Method for Large Scale Optimization. *Math. Program.* **1989**, *45*, 503–528.

- (9) Kingma, D. P.; Welling, M. Auto-Encoding Variational Bayes. Proceedings of the 2nd International Conference on Learning Representations. 2014.
- (10) Gilmer, J.; Schoenholz, S. S.; Riley, P. F.; Vinyals, O.; Dahl, G. E. Neural Message Passing for Quantum Chemistry. Proceedings of the 34th International Conference on Machine Learning. 2017; pp 1263–1272.
- (11) Scarselli, F.; Gori, M.; Tsoi, A. C.; Hagenbuchner, M.; Monfardini, G. The Graph Neural Network Model. *IEEE Trans. Neural Netw.* **2009**, *20*, 61–80.
- (12) Bruna, J.; Zaremba, W.; Szlam, A.; LeCun, Y. Spectral Networks and Locally Connected Networks on Graphs. Proceedings of the 2nd International Conference on Learning Representations. 2014.
- (13) Cho, K.; Van Merriënboer, B.; Gulcehre, C.; Bahdanau, D.; Bougares, F.; Schwenk, H.; Bengio, Y. Learning Phrase Representations Using RNN Encoder-Decoder for Statistical Machine Translation. Proceedings of the 2014 Conference on Empirical Methods in Natural Language Processing. 2014; pp 1724–1734.
- (14) Pearl, J. Fusion, Propagation, and Structuring in Belief Networks. *Artif. Intell.* **1986**, *29*, 241–288.
- (15) Ruddigkeit, L.; Van Deursen, R.; Blum, L. C.; Reymond, J.-L. Enumeration of 166 Billion Organic Small Molecules in the Chemical Universe Database GDB-17. *J. Chem. Inf. Model.* **2012**, *52*, 2864–2875.
- (16) Ramakrishnan, R.; Dral, P. O.; Rupp, M.; Von Lilienfeld, O. A. Quantum Chemistry Structures and Properties of 134 Kilo Molecules. *Sci. Data* **2014**, *1*, 140022:1–7.
- (17) Gražulis, S.; Daškevič, A.; Merkys, A.; Chateigner, D.; Lutterotti, L.; Quiros, M.; Serebryanaya, N. R.; Moeck, P.; Downs, R. T.; Le Bail, A. Crystallography Open

- Database (COD): An Open-Access Collection of Crystal Structures and Platform for World-Wide Collaboration. *Nucleic Acids Res.* **2012**, *40*, D420–D427.
- (18) Groom, C. R.; Bruno, I. J.; Lightfoot, M. P.; Ward, S. C. The Cambridge Structural Database. *Acta Crystallogr. Sect. B-Struct. Sci.Cryst. Eng. Mat.* **2016**, *72*, 171–179.
- (19) Weininger, D. SMILES, A Chemical Language and Information System. 1. Introduction to Methodology and Encoding Rules. *J. Chem. Inf. Comput. Sci.* **1988**, *28*, 31–36.
- (20) Hautier, G.; Jain, A.; Ong, S. P. From the Computer to the Laboratory: Materials Discovery and Design Using First-Principles Calculations. *J. Mater. Sci.* **2012**, *47*, 7317–7340.
- (21) Srivastava, N.; Hinton, G.; Krizhevsky, A.; Sutskever, I.; Salakhutdinov, R. Dropout: A Simple Way to Prevent Neural Networks from Overfitting. *J. Mach. Learn. Res.* **2014**, *15*, 1929–1958.
- (22) Kingma, D. P.; Ba, J. Adam: A Method for Stochastic Optimization. Proceedings of the 3rd International Conference on Learning Representations. 2015.
- (23) Ratcliff, L. E.; Mohr, S.; Huhs, G.; Deutsch, T.; Masella, M.; Genovese, L. Challenges in Large Scale Quantum Mechanical Calculations. *Wiley Interdiscip. Rev.-Comput. Mol. Sci.* **2017**, *7*, e1290.
- (24) Hawkins, P. C. D. Conformation Generation: The State of the Art. *J. Chem. Inf. Model.* **2017**, *57*, 1747–1756.
- (25) Kearnes, S.; McCloskey, K.; Berndl, M.; Pande, V.; Riley, P. Molecular Graph Convolutions: Moving Beyond Fingerprints. *J. Comput.-Aided Mol. Des.* **2016**, *30*, 595–608.
- (26) Ramsundar, B.; Eastman, P.; Leswing, K.; Walters, P.; Pande, V. *Deep Learning for the Life Sciences*; O'Reilly Media, 2019.